Composites Part B 225 (2021) 109268

Contents lists available at ScienceDirect

Composites Part B

journal homepage: www.elsevier.com/locate/compositesb

Coaxial direct ink writing of shear stiffening gel/Ecoflex composite for customized insoles

Shuaishuai Zhang [a], Liang Lu [b,**], Sheng Wang [a], Fang Yuan [a], Shouhu Xuan [a,***], Xinglong Gong [a,*]

[a] CAS Key Laboratory of Mechanical Behavior and Design of Materials, Department of Modern Mechanics, University of Science and Technology of China (USTC), Hefei, Anhui, 230027, PR China

[b] The First Affiliated Hospital of USTC, Division of Life Sciences and Medicine, University of Science and Technology of China, Hefei, Anhui, 230036, PR China

ARTICLE INFO

Keywords:
A. Smart materials
A. Polymer-matrix composites (PMCs)
B. Rheological properties
B. Impact behavior
E. Extrusion

ABSTRACT

Traditional sports insoles could reduce plantar pressure and protect against external dynamic shock during exercising, while their performance was limited severely for individuals with abnormal gait. Thus, it was in urgent need to develop insoles with both safeguarding and orthopedic functions. Here, shear stiffening gel (SSG), whose storage modulus rose dramatically with the shear frequency, was encapsulated in elastic elastomer (Ecoflex) tubes by using the coaxial direct ink writing technique to prepare customized insoles. The printing parameters were investigated to optimize the mechanical property of SSG/Ecoflex composite core-sheath fibers and hybrid films. Due to the rate-dependent mechanical property of inner SSG, the hybrid films could dissipate 53.4% impact acceleration, 46.9% penetrated force and increase buffer time by 1.6 times under dynamic loadings, thus presenting excellent safeguarding performance. Compared with commercial insoles, coaxial additive manufactured SSG/Ecoflex hybrid insoles not only exhibited better protection against sudden shocks during mild and violent exercises but also provided physical corrections to abnormal walking gaits, such as varus and valgus foot. Therefore, the programmable coaxial additive manufacture technique for constructing SSG/Ecoflex composite sports armors hold great promise for future advanced safeguarding and customized health improvement.

1. Introduction

Due to the increasing security requirements of policing issues and confrontational sports, it is an emergency task to develop the body armors to protect against external violent shocks [1–4]. Shear stiffening gel (SSG), whose storage modulus increases 3–4 orders of magnitude with the increase of shear frequency, has been wildly researched owing to the excellent performance of energy absorption and stress dissipation [5–8]. The typical rate-dependent property endowed SSG with superior anti-impact performance, which reduced the peak penetrated stress by 2 orders of magnitude [9]. Due to the perspective in personal protection areas, SSG was impregnated into Kevlar fabrics for preparing soft armors which could reduce 49.5% impact force and dissipate 21.6% impact energy [10]. However, the cold-flow behavior of SSG originated from the highly viscoelastic nature suppressed its further practical applications severely [11]. Various physical operations were employed to resist this disadvantage, such as impregnating SSG into porous polyurethane sponge [12] or packaging SSG within soft silicone elastomer [13]. But these methods suffered from a complicated process, high cost, or uncontrollability, which seriously restricted the development of SSG-based sports armors. Besides, individuals with physical diseases or abnormal gaits require additional external assistance [14,15], while producing custom-tailored products for end-users is a huge challenge for traditional manufacturing methods due to the high costs.

The emerging additive manufacture (AM, also referred to as 3D printing) technique with the advantages of scalability and controllability has provided a new strategy for constructing customized products and complex structures simply in a programmable manner [16–19]. The AM technique has been successfully applied in many areas such as sensors [20–22], microfluidic networks [23], photonic bandgap

* Corresponding author.
** Corresponding author.
*** Corresponding author.
E-mail addresses: luliangzhwk@163.com (L. Lu), xuansh@ustc.edu.cn (S. Xuan), gongxl@ustc.edu.cn (X. Gong).

https://doi.org/10.1016/j.compositesb.2021.109268
Received 27 May 2021; Received in revised form 16 August 2021; Accepted 27 August 2021
Available online 28 August 2021

materials [24], tissue scaffolds [25,26], and drug delivery devices [27,28]. The common ways for printing polymers [29–32] are composed of direct ink writing (DIW), fused deposition modelling (FDM), stereolithography (SLA) and so on. Among them, DIW is the most versatile AM technique in terms of materials development, which enables the creation of complex 3D shapes by formulating a paste with controlled rheology [33,34]. More importantly, DIW enables a combination of different formulations into complex structures by using multiple extrusion nozzles in previously inaccessible or infeasible ways [35]. For example, typical methods of developing protective elastomer sheath include wrapping prestretched polymer fibers with elastic species [36], or encapsulating a liquid or gel in an elastomer by stencil printing, injection into microchannels, and droplet deposition [37,38]. The coaxial DIW technique provided a scalable approach to fabricate core-sheath structures in a feasible and programmable manner [39–42]. Liquid metal could be directly encapsulated into an elastomeric sheath in a single step without any post-processing such as injecting or casting by coaxial DIW technique [43]. Moreover, Zhao successfully applied coaxial DIW technique in the fabrication of coaxial fiber-shaped supercapacitors and energy storage devices [44–46]. Besides, the fibrous supercapacitors fabricated coaxial DIW technique exhibited excellent long-term cycling performance with capacitance retention of 98.63% after 12,000 cycles [47]. Therefore, the coaxial DIW technique may be a good choice to package highly viscoelastic SSG into elastic sheath for the preparation of steady and customized sports armors.

In this work, the coaxial DIW technique was developed to prepare SSG/Ecoflex composites based customized insoles. A coaxial nozzle was applied to extrude the inner printing ink (SSG) and outer printing ink (liquid Ecoflex) simultaneously, in which viscoelastic SSG was encapsulated within an elastic tube. The printing parameters were investigated to improve the rheological property of SSG/Ecoflex composite core-sheath fibers and the further developed SSG/Ecoflex hybrid films. The printing direction induced the tensile anisotropy of the printed films, which could be improved by designing the printing direction of the double-layer films. Due to the rate-dependent property of inner SSG, the films could dissipate impact acceleration and penetrated force effectively under dynamic loadings. With the help of the scalable coaxial DIW technique, customized insoles were prepared in a feasible and programmable manner. They could not only dissipate dynamic force and protect the foot more effectively compared with commercial insoles during exercises, but also provide physical correction to the abnormal walking gait, such as varus and valgus foot. Thus, the coaxial additive manufacture technique based on SSG/Ecoflex composites had broad application prospection in customized sports armors with both safeguarding and health improvement functions.

2. Experiment section

2.1. Materials

Ethanol and boric acid were all purchased from Sinopharm Chemical Reagent Co. Ltd., Shanghai, China. Hydroxyl silicone oil (PDMS, 500 mm^2/s, AR degree, from Jining Huakai Resin Co., Ltd) was used to prepare shear stiffening gel (SSG). Commercially available silicone elastomer Ecoflex 00–20, Thi-Vex Silicone Thickener and Slo-Jo Platinum Silicone Cure Retarder were purchased from Smooth-On (Macungie, PA, USA).

2.2. Preparation of printing inks

By consciously stirring for 10 min, 1 g boric acid and 40 mL hydroxyl silicone oil were mixed evenly in a ceramic dish. Then, the mixture was heated at 180 °C for 1.5 h and was stirred every 15 min to ensure the homogeneous reaction. The mixture formed lightly cross-linked, sticky and viscous gel during the heating process. After cooling to room temperature, the core ink (SSG) was obtained.

10 g Ecoflex 00–20 Part A with 10 g Part B were mixed homogeneously. Then, 0.5 g Thi-Vex Silicone Thickener (referred to as Thi) was added as rheological modifier and 0.2 g Slo-Jo Platinum Silicone Cure Retarder was applied to increase the pot life. After that, the mixture was thoroughly stirred and degassed in a planetary centrifugal mixer (HM800, Shenzhen Hasai Technology Co., Ltd., Shenzhen, China) at 3000 rpm for 15 min. Finally, the obtained sheath ink was transferred to a 20 mL syringe.

2.3. Printing of SSG/Ecoflex composite core-sheath fiber and SSG/Ecoflex hybrid film

The coaxial nozzles were constructed by using an Object260 Connex3 PloyJet 3D multi-material printer (Statasys Ltd.). The outlet diameters of the inner and outer nozzle were 0.6 and 1.0 mm, respectively (Fig. 1b). The inner nozzle could be screwed into the outer nozzle tightly and form coaxial channels for printing inks flowing in the desired configuration. A 20 mL pneumatic syringe was used to store the core ink (SSG). An air cylinder connected to an air compressor and a pressure regulator (XN2010, Puma Industrial Co., Ltd.) were used to provide 0.6 MPa air pressure to extrude SSG through the inner nozzle. The printing speed was set at 30 mm/min. A syringe pump (LSP02-1B, Longer Pump Co., Ltd.) was adopted to control the extrusion speed of the sheath ink (liquid Ecoflex) through the outer nozzle (Figs. 1a and S1). All experiments were carried out at room temperature (25 °C).

The coaxial nozzle was assembled on a computer-controlled 2-axis movement platform (VG-L5S, Vigotec Co., Ltd.). The printing paths were designed by using 2D models (constructed by SolidWorks, MA, USA) and complied with Vigo-Engravel software. The SSG/Ecoflex composite core-sheath fibers were printed on even polyethylene terephthalate (PET) films at 30 mm/min (Fig. 1c). The SSG/Ecoflex hybrid films were constructed by printing parallel fibers with an interval of 1.25 mm. Then, the SSG/Ecoflex hybrid films were vulcanized in an oven at 80 °C for 15 min and peeled off from the PET films to obtain final products (Fig. 1d).

2.4. Characterization

The rheological properties of the inks were characterized using a stress-controlled rheometer (Physica MCR302, Anton Paar Co., Austria). The samples, molded into a cylinder shape with a thickness of 1 mm and diameter of 20 mm, were tested with a parallel plate (diameter: 20 mm). At the frequency sweep tests, the strain was set at 0.1%. At the strain sweep tests, the shear frequency was set at 1 Hz. The above tests were carried out at 25 °C. The images were taken by digital microscope (KEYENCE VHX Digital Microscope, VH-Z100). The stretch tests were carried out by using a dynamic mechanical analyzer (DMA, Electro Force 3200, TA instruments, Minnesota 55344 USA). The length and width of samples were 40 and 5 mm, respectively. The impact tests were carried out with a drop tower machine (ZCJ1302-A, MTS System Co., America) with the drop hammer mass of 0.25 kg and 0.50 kg. The side length of square samples was 40 mm. The plantar pressure was collected by using pressure sensitive paper (Prescale, 4LW, Fujifilm Holdings Co., Japan). The dynamic impact tests and plantar pressure tests were carried out at room temperature.

3. Results and discussion

3.1. Rheological properties of printing inks

Shear stiffening gel (SSG) was a kind of lightly crosslinked polyborosiloxane polymer material with unique rate-dependent mechanical properties. In natural state, SSG was soft and plastic with low modulus, which was prone to exhibit irrecoverable plastic deformation under external force or gravity. Upon external loads with high strain rate, SSG transformed from the viscous liquid state to rubbery state and glassy

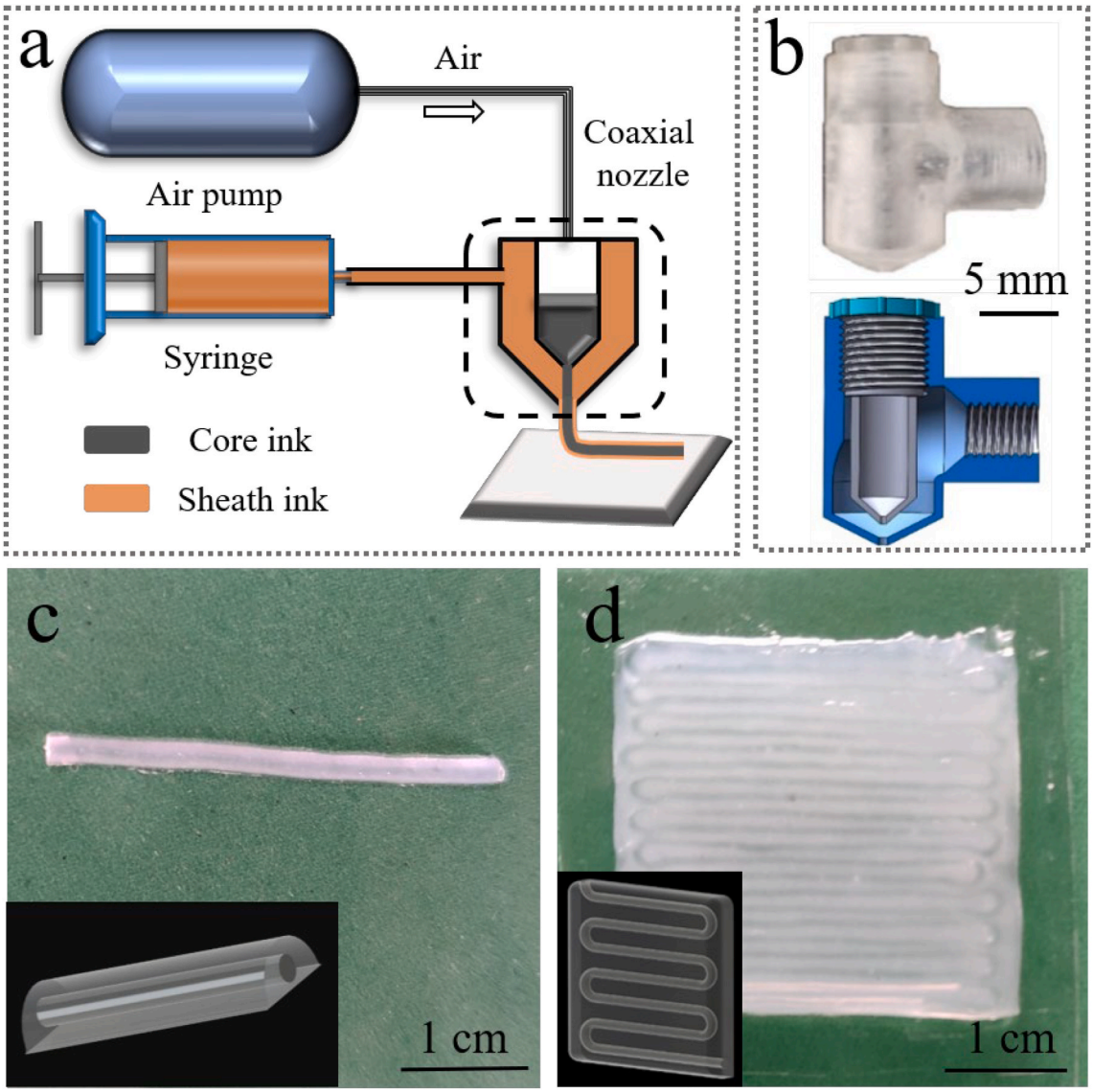

Fig. 1. The schematic of coaxial DIW devices (a). The coaxial nozzle and its cross-sectional schematic diagram (b). The images and schematics of SSG/Ecoflex composite core-sheath fiber (c) and SSG/Ecoflex hybrid film (d).

state quickly [48,49]. The dynamic oscillatory shear tests were applied to illustrate the typical shear stiffening property of SSG (Fig. 2a). At 0.1 Hz, the storage modulus of SSG was only 92 Pa, which was much lower than the loss modulus (3826 Pa). As the shear frequency rose to 100 Hz, its storage modulus increased by 3 orders of magnitude to 0.23 MPa sharply, which demonstrated that SSG presented a hard solid-state behavior. The creep behavior of SSG was characterized by applying shear stress of 10 Pa for 300 s and then the shear stress was removed at the following 600 s (Fig. 2b). The shear strain increased almost linearly with time at 10 Pa shear stress. At 300 s, the shear strain reached 56.7%. The shear strain was composed of two parts: elastic and plastic. After removing the external loadings, the elastic strain disappeared, and the remaining part that could not be restored was the plastic strain. Apparently, the shear strain decreased slightly with an unrecoverable strain of 55.8% at 900 s as the shear stress returned to 0. Thus, SSG presented strong plastic nature and could not recover its initial state after being subject to external loadings.

To demonstrate the cold-flow behavior of SSG in a visible way, the creep tests were carried (Fig. 2c). SSG was cut into a rectangle shape (length: 55 mm, height: 8 mm, width: 15 mm). Then, the both sides were placed on the steps with the middle part hanging in the air. The hanging distance was 30 mm. The middle part collapsed and fell down under gravity. Finally, the middle part ruptured and dropped onto the ground at 450 s. Due to the low cross-linking density of polymer chains, SSG behaved as a liquid and could not maintain a stable shape in the natural state. Thus, it was necessary to encapsulate SSG into elastic sheath for practical applications.

The relationship between the modulus and the shear strain was investigated to study the printability of SSG (Fig. 2d). The shear frequency was set at 1.0 Hz. The storage and loss modulus of SSG kept stable at low strain and tended to fall as the shear strain increased. Here, the yield strain was about 40%. The loss modulus was larger than the storage modulus. Thus, SSG exhibited a liquid-like nature and tended to flow at static state, indicating that SSG could be extruded from the nozzle.

The viscosity of the liquid Ecoflex was independent of the shear rate (Fig. 2e). With the introduction of the rheology modifier (Thi), its viscosity decreased with strain rate, presenting shear thinning property. The viscosity, the ratio of shear stress and shear rate, reflected the resistance of the fluid to the flow. Low viscosity at high strain rate benefited the smooth flow of sheath ink through the nozzle. After the fiber was extruded onto the substrate, the high viscosity at static state

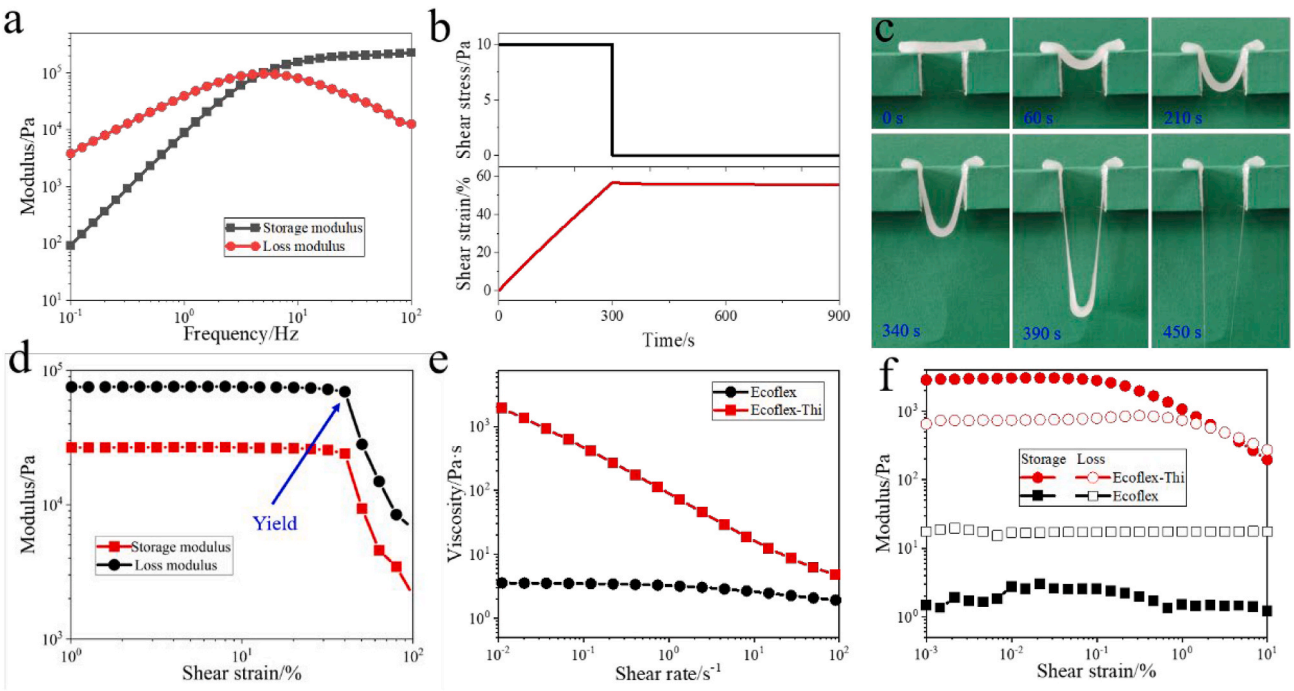

Fig. 2. The rheological properties of printing inks. The storage and loss modulus of SSG plotted versus shear frequency (a). The creep behavior of SSG under 10 Pa shear stress (b). The cold-flow behavior of SSG under gravity (c). The storage and loss modulus of SSG plotted versus shear strain (d). The viscosity (e) and storage, loss modulus (f) of liquid Ecoflex.

suppressed its shape change. Thus, the shear-thinning feature benefited the core-sheath fiber fabrication during the coaxial DIW experiments. The modulus of the liquid Ecoflex was irrelevant with the shear strain and the loss modulus was larger than its storage modulus, presenting a liquid-like behavior (Fig. 2f). The addition of rheological modifier (Thi) improved the printability of liquid Ecoflex apparently. The storage modulus of Ecoflex-Thi reached 2850 Pa which was much higher than the corresponding loss modulus at low strain. This result indicated that Ecoflex-Thi presented a solid-like characteristic, which was essential for the shape retention of the SSG/Ecoflex composite core-sheath fibers. Moreover, the low yield and sol-gel transition shear strain assisted the fluent extrusion through the coaxial nozzle. In conclusion, Ecoflex-Thi was a suitable printing ink for the following coaxial DIW experiments.

3.2. Morphology characterization of SSG/Ecoflex composite core-sheath fibers and SSG/Ecoflex hybrid films

SSG/Ecoflex composite core-sheath fibers with different sizes could be obtained by adjusting the sheath extrusion speed (Fig. 3a). The core-sheath fiber presented a semicircular shape. During the printing process, the core SSG and sheath liquid Ecoflex were coextruded from the nozzle and both formed circular shapes at first. The static modulus of SSG was much larger than sheath liquid Ecoflex. Thus, liquid Ecoflex was deposited on the printing platform due to gravity and formed a semi-circle shape quickly. The deformation in SSG was much slower. Moreover, the static storage modulus of liquid Ecoflex was larger than loss modulus and it could support inner SSG, which hinder the further deformation in SSG. Thus, the core SSG maintained the initial circular shape. The cylindrical SSG was at the center of the fiber and completely wrapped by Ecoflex. With the increase of sheath extrusion speed, the fiber shape almost unchanged, while the cross-sectional area increased obviously due to the growing outer layer (Fig. 3c). As the sheath extrusion speed rose from 0.4 to 0.6 mm^3/s, the sheath area enlarged from 1.32 to 1.90 mm^2. The sheath area was much larger than the exit area of the coaxial nozzle (0.785 mm^2). This was mainly induced by the die swelling phenomenon [50,51]. After being transferred into the nozzle, the printing inks were strongly squeezed. Although the deformation was relaxed when flowing inside the nozzle, a large amount of internal stress remained. When the printing inks lost the restraint at the exit, elastic recovery occurred, resulting in die swelling. As the sheath extrusion speed was set at 0.6 mm^3/s, the average core area and sheath area were 0.36 and 1.90 mm^2, respectively. The corresponding standard deviations were 0.065 and 0.14 mm^2, respectively. The low standard deviations demonstrated the good geometrical accuracy of the printed core-sheath fibers. Moreover, the air pressure was varied to optimize the structure of the core-sheath fiber (Fig. S2).

The SSG/Ecoflex hybrid film was obtained by printing fibers in parallel and the distance between adjacent fibers was kept at 1.25 mm (Fig. 3b). The films were flat and the cylindrical SSG was evenly spaced inside the films. When the sheath extrusion speed was 0.4 mm^3/s, the encapsulation effect of Ecoflex on the inner SSG was poor. The thickness of the films increased with the sheath extrusion speed (Fig. 3d). Raising the sheath extrusion speed from 0.4 to 0.6 mm^3/s, the thickness of the film enlarged from 1.18 to 1.37 mm. As the sheath extrusion speed overpassed 0.6 mm^3/s, the sheath Ecoflex could encapsulate the inner SSG tightly and thoroughly.

3.3. Mechanical properties of the SSG/Ecoflex hybrid films

Due to the shear stiffening characteristics of SSG, the SSG/Ecoflex hybrid films also presented a rate-dependent mechanical property (Fig. 4a). For example, as the sheath extrusion speed was set at 0.5 mm^3/s, the storage modulus of SSG/Ecoflex hybrid film at 0.1 Hz was 6.5 kPa and increased quickly to 17.4 kPa at 10 Hz. The storage modulus of the films increased with the sheath extrusion speed. At 0.1 Hz, the storage modulus increased from 6.5 to 13.8 kPa as the sheath extrusion speed rose from 0.5 to 1.0 mm^3/s. Because of the elasticity of the Ecoflex sheath, the SSG/Ecoflex hybrid films behaved differently in the creep tests (Fig. 4b). Ecoflex film underwent 0.84% elastic deformation within 0.1 s under a shear stress of 100 Pa. Then the shear strain stabilized at about 0.94% until 100 s. After removing the shear stress, the shear strain reduced to 0.2% in 1 s, and then declined to almost 0 in the following 50

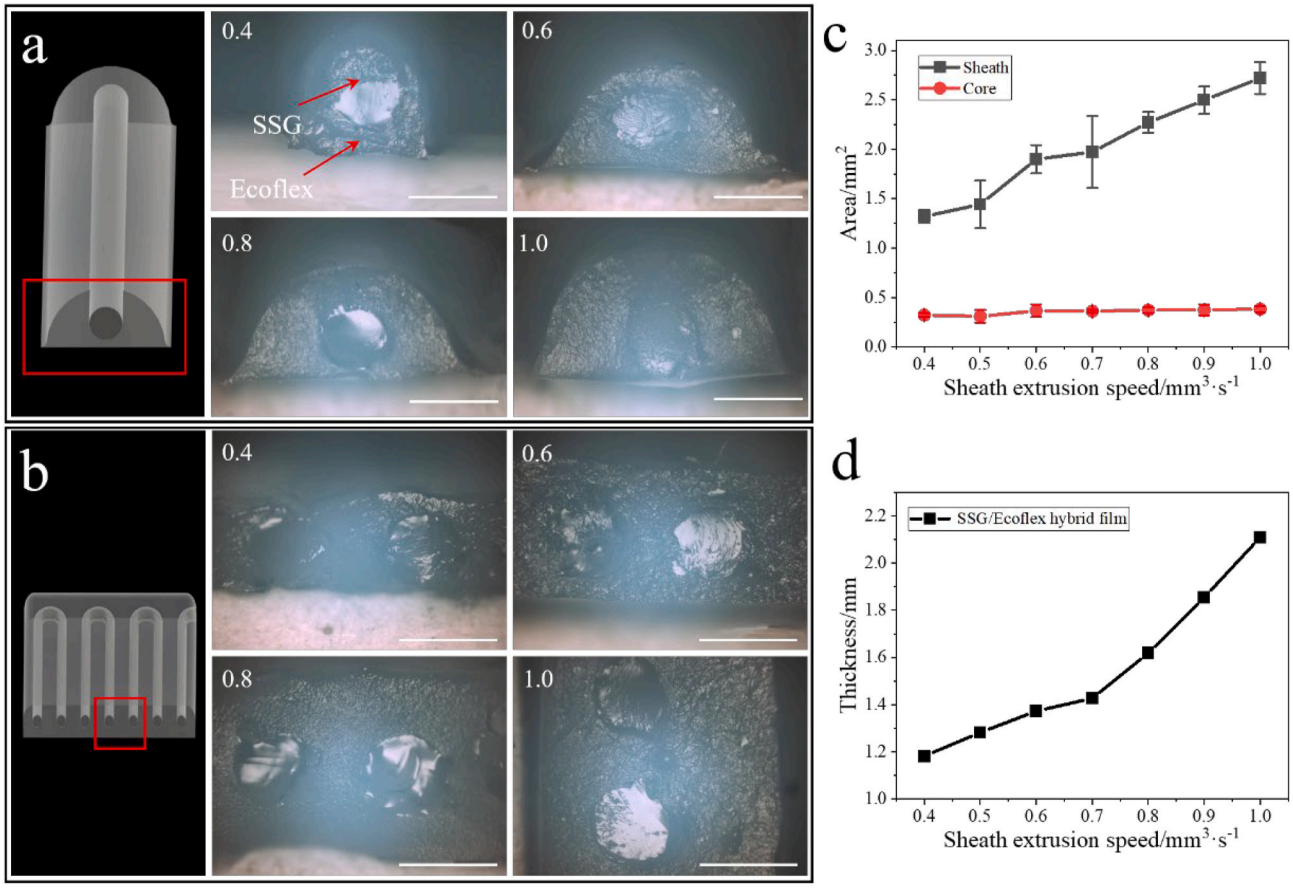

Fig. 3. The morphology of SSG/Ecoflex composite fibers and SSG/Ecoflex hybrid films. The schematic and section view of SSG/Ecoflex composite fibers (a) and SSG/Ecoflex hybrid films (b) at different sheath extrusion speed of 0.4, 0.6, 0.8, 1.0 mm^3/s, respectively. The red frame showed the shooting area and the scale bar was 1 mm. The fiber area plotted vs sheath extrusion speed (c). The film thickness as a function of sheath extrusion speed (d). (For interpretation of the references to colour in this figure legend, the reader is referred to the Web version of this article.)

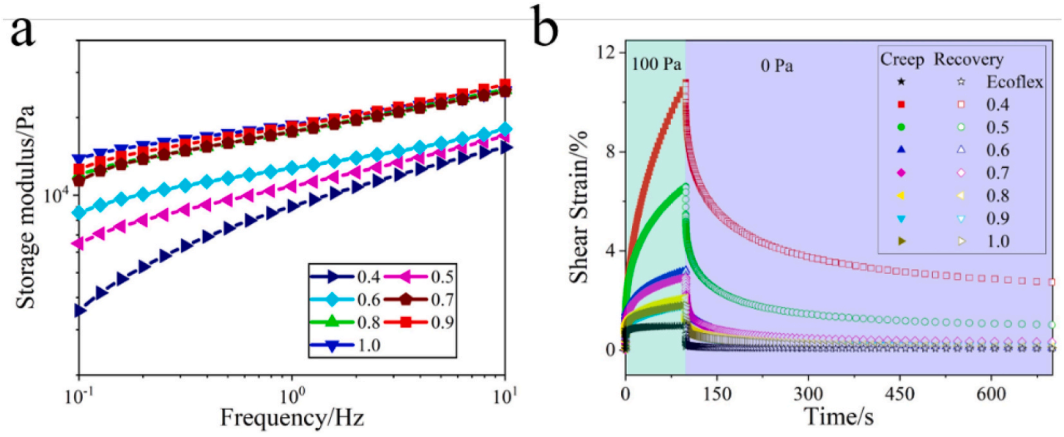

Fig. 4. The storage modulus (a) and creep behavior (b) of SSG/Ecoflex hybrid films with different sheath extrusion speed.

s. Ecoflex film could return to its original state quickly, showing excellent elastic recovery property. The elastic Ecoflex sheath also benefited the mechanical stability of core-sheath films. As the sheath extrusion speed was 1.0 mm^3/s, the shear strain of SSG/Ecoflex hybrid film reached 1.8% at 100 Pa shear stress. After removing the external force, the shear strain recovered to 0.2% at 234 s, showing a weaker recovery ability. The residual shear strain at 900 s was less than 0.1%, which meant the film could finally return to the original state. As the sheath extrusion speed reduced, the SSG percentage increased. Thus, the viscoelasticity of the SSG/Ecoflex hybrid film became stronger gradually. The deformation in the creep stage (green part) increased and the mechanical recovery ability reduced accordingly. However, when the sheath extrusion speed overpassed 0.5 mm^3/s, SSG/Ecoflex hybrid films could recover completely with the residual strains less than 0.1% at 900 s. Moreover, the inner SSG could be encapsulated into the outer Ecoflex sheath completely as the sheath extrusion speed was larger than 0.5 mm^3/s. The printing condition with 0.6 mm^3/s sheath extrusion speed was good enough to meet the experimental requirements and was

selected as the optimum for the following experiments.

As shown in Fig. 5a, the film exhibited strong anisotropy due to the horizontal printing direction. Compared with the 'Y–Y' direction, the tensile stress was much larger in the 'X-X' direction. Moreover, the tensile elongation in the 'X-X' direction was 717%, while in the 'Y–Y' direction was only 528%. The anisotropy could be regulated by adjusting the printing direction of double-layer films. The printing direction angle of the top layer with the bottom layer was set at 30°, 45° and 90°, respectively (Fig. 5b–d). As the printing direction angle increased, the difference of the stress-strain curves in the 'X-X' direction and 'Y–Y' direction gradually decreased. When the printing direction angle rose to 90°, the tensile mechanical behaviors were almost identical. The modulus of SSG was low in the natural state. Under quasi-static stretch, the tensile stress was mainly originated from the Ecoflex layer. The Ecoflex proportion along the 'X-X' direction was much larger than the 'Y–Y' direction, which resulted in the stress and tensile elongation difference. As the printing direction angle increased, the difference of the Ecoflex proportion in two directions gradually reduced to 0, leading to almost identical stress at 100% strain and tensile elongation (Fig. S3).

Due to the shear stiffening characteristics of SSG, SSG/Ecoflex hybrid monolayer film could absorb dynamic impact energy and force under dynamic loadings, exhibiting effective protection against external shocks. The impact tests were carried out to evaluate its protective performance with a drop hammer mass of 0.25 kg. The acceleration sensor was placed on the drop hammer to record the impact acceleration signals and the force sensor was deposed under the film to collect the penetrated force signals. Besides, the drop hammer impacting on the force sensor without a protective layer was used as reference, and SSG and Ecoflex films with the same thickness were applied as the comparison. At 0.1 m drop height, when the drop hammer directly impacted upon the force sensor, the acceleration signal increased sharply and reached the peak value (6.95 km/s^2) within 0.28 ms (Fig. 6a). Meanwhile, the drop hammer velocity was reduced to zero and this time was called buffer time. The impact energy was released during the buffer time and a shorter buffer time could cause greater damage. The penetrated force increased with the impact acceleration signal accordingly and reached a peak value of 648 N at 0.28 ms (Fig. 6b). After that, the drop hammer began to rebound back, leading to the reduction of impact acceleration and penetrated force. Then, the drop hammer impacted upon the force sensor again at 1.7 ms, resulting in the second peak.

Compared with other samples, the impact acceleration and penetrated force of SSG films were the smallest, presenting superior safeguarding performance. At 0.1 m drop height, the peak impact acceleration was reduced from 6.95 to 2.16 km/s^2 as SSG film was applied. SSG damped out the impact force effectively owing to the shear-stiffening effect. Besides, the buffer time was enlarged from 0.28 ms to 1.21 ms, which benefited the force and energy dissipation. As the drop hammer stroked on SSG film, shear stiffening effect occurred and the dramatic increase of the rate-dependent rigidity could endure and damp out the impact force effectively [9,52]. The peak impact accelerations of Ecoflex and SSG/Ecoflex hybrid film were 3.60 and 2.47 km/s^2, respectively. Compared with Ecoflex film, SSG/Ecoflex hybrid film could reduce the peak impact acceleration by 31.0%. Moreover,

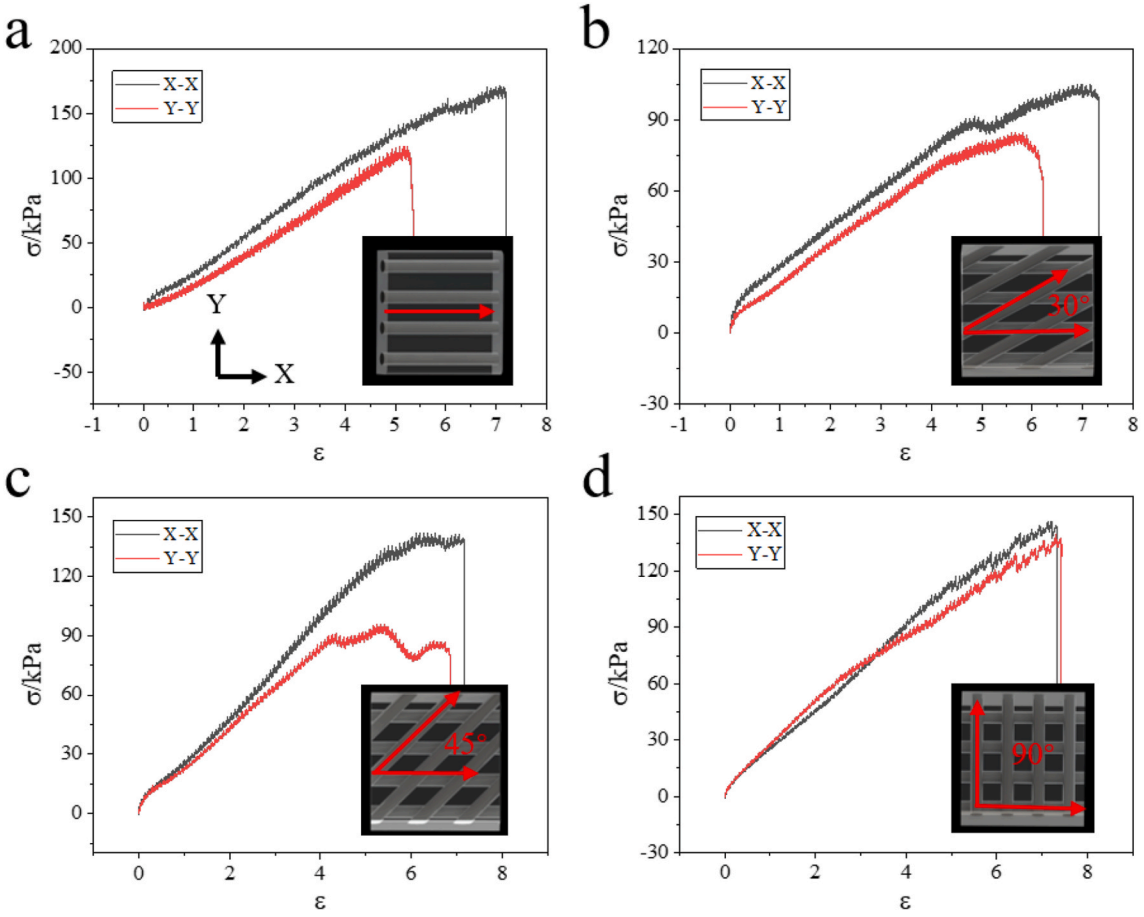

Fig. 5. The quasi-static tensile properties of the SSG/Ecoflex hybrid films. The stress-strain curves of the monolayer film when stretched in different directions (a). The tensile stress-strain curves in different directions as the printing direction angles of the double-layer films were 30° (b), 45° (c) and 90° (d), respectively. The red arrows exhibited the printing directions of double-layer films. (For interpretation of the references to colour in this figure legend, the reader is referred to the Web version of this article.)

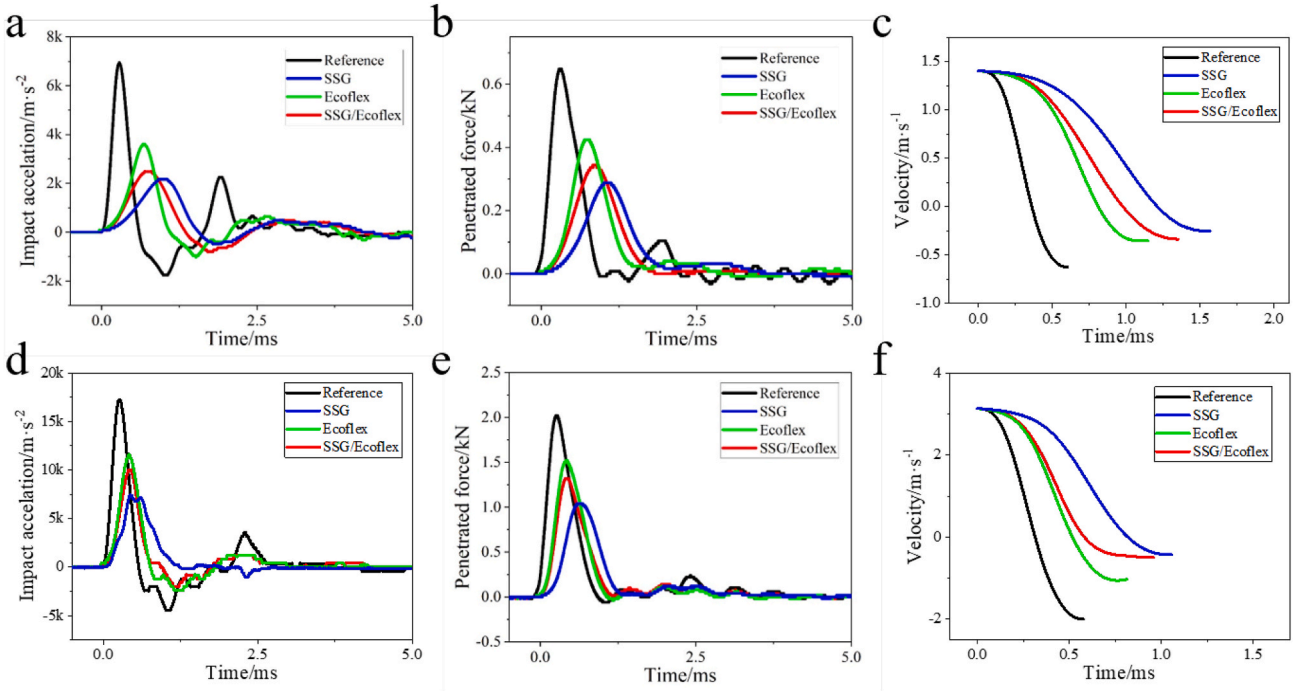

Fig. 6. The anti-impact performance of the SSG/Ecoflex hybrid monolayer film. The impact acceleration signals of drop hammer (a, d) and penetrated force (b, e) during the impact process at the drop height of 0.1 and 0.5 m, respectively. The velocity of drop hammer at the drop height of 0.1 (c) and 0.5 m (f).

SSG/Ecoflex hybrid film could reduce penetrated force by 18.8% compared with Ecoflex film. Thus, the introduction of SSG enhanced the safeguarding performance of Ecoflex film dramatically.

By integrating the impact acceleration signals, the velocity of drop hammer during the impact process was obtained (Fig. 6c). As the drop hammer impacted upon the force sensor directly, its velocity dropped quickly to zero. The impact energy was released in a short time, which would result in tremendous damage to the human body. Then, the hammer rebounded back at a velocity of 0.62 m/s, which resulted in the second shock. As the SSG/Ecoflex hybrid film was applied, the velocity of drop hammer reduced much slower and the rebound velocity was declined to 0.33 m/s, avoiding unwanted second harm. As the drop height increased to 0.5 m, the SSG film also exhibited the smallest impact acceleration and penetrated force due to the excellent force dissipation property of SSG (Fig. 6d and e). Similarly, the anti-impact behavior of SSG endowed SSG/Ecoflex hybrid film with lower impact acceleration and penetrated force compared with Ecoflex film. Besides, the rebound velocity of Ecoflex film was 1.04 m/s, which was further reduced to 0.50 m/s by SSG/Ecoflex hybrid film, presenting excellent energy dissipation capability of inner SSG.

The values of peak impact acceleration and penetrated force, buffer time and rebound velocity evidenced the superior safeguarding behavior against dynamic shocks of SSG (Fig. S4). The dynamic 'B–O' bonds between different chains in SSG were the main reason for the rate-dependent mechanical property [49]. The dynamic bonds could break and reform with time, connecting the polymer chains into a uniform network structure. In natural state, the dynamic bonds had enough time to break and reform slowly, giving the polymer network certain mobility. The slight friction between polymer chains bear most of the external force. In this case, SSG was soft, plastic and easy to deform. At high strain rate, a large number of dynamic bonds had no enough time to break, locking the whole polymer network. Thus, SSG modulus increased sharply and undertook dynamic force. Consequently, SSG transformed from viscous liquid state to rubbery state and produced a large number of microcracks, which effectively absorbed the impact energy and buffered the impact force [12]. However, SSG possessed a typical cold-flow behavior in natural state, which hindered its further applications. SSG/Ecoflex hybrid film not only possessed outstanding protection performance but also resisted the flow nature of SSG effectively. After being impacted, SSG/Ecoflex hybrid film could return to its original state quickly, which expanded its application prospect and value in the field of buffer protection such as soft armor and cushioning area.

The printing direction of SSG/Ecoflex hybrid double-layer film influenced its anisotropy in quasi-static state, so the effect of the printing direction on the performance under dynamic impact attracted our interest. As shown in Fig. 7, the penetrated force signals at drop heights of 0.1 m and 0.5 m exhibited almost identical regardless of the printing direction angle. The anisotropy of SSG/Ecoflex hybrid double-layer film was located in the 'X–Y' plane, and the dynamic impact force was perpendicular to this plane. Therefore, the printing direction of double-layer films was irrelevant to the anti-impact performance.

3.4. The application of SSG/Ecoflex hybrid films in insoles

During exercises, human feet will be subject to huge pressure. Without necessary protection, injuries such as sprains and ligaments torn are prone to occur [53,54]. Due to the excellent dynamic anti-impact performance, the SSG/Ecoflex hybrid film insoles were printed to protect the human foot. The insoles were composed of three layers of SSG/Ecoflex hybrid films with printing directions of 0°, 90° and 0° (Fig. 8a). The size of the insoles was 8.0 cm × 24.0 cm. A 0.5 kg drop hammer was used to conduct impact tests at different drop heights to analyze the dynamic cushioning effect of the insoles. Traditional materials for commercial insoles, such as EVA foam and Poron foam, were tested as comparison.

Without protection, the penetrated force reached 3.92 kN at a drop height of 10 cm (Fig. 8b). The large and destructive impact force would result in great injuries to human feet, ankles and muscles. The application of insoles significantly reduced the penetrated force by about an order of magnitude, providing effective protection to the sole skin and tissues during intense exercises. To analyze and compare the buffer effect, the buffer ratio of each insole was calculated as

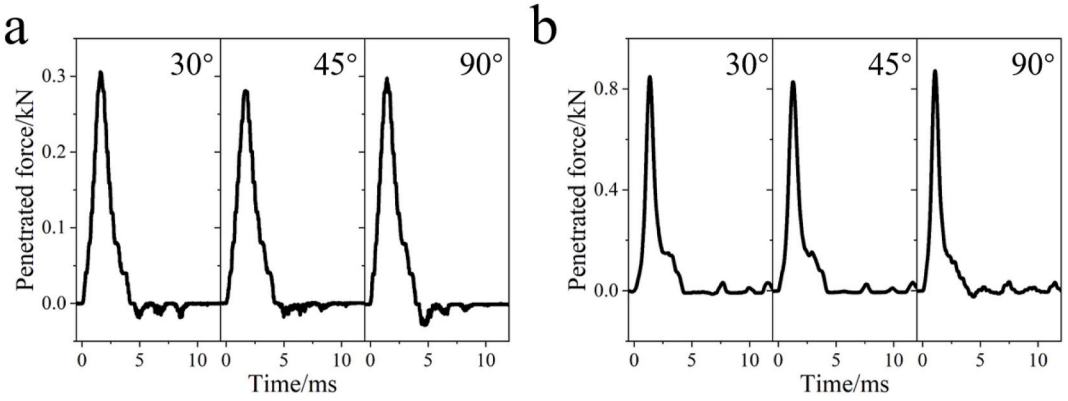

Fig. 7. The penetrated force of SSG/Ecoflex hybrid double-layer films with different printing degrees at the drop height of 0.1 (a) and 0.5 m (b).

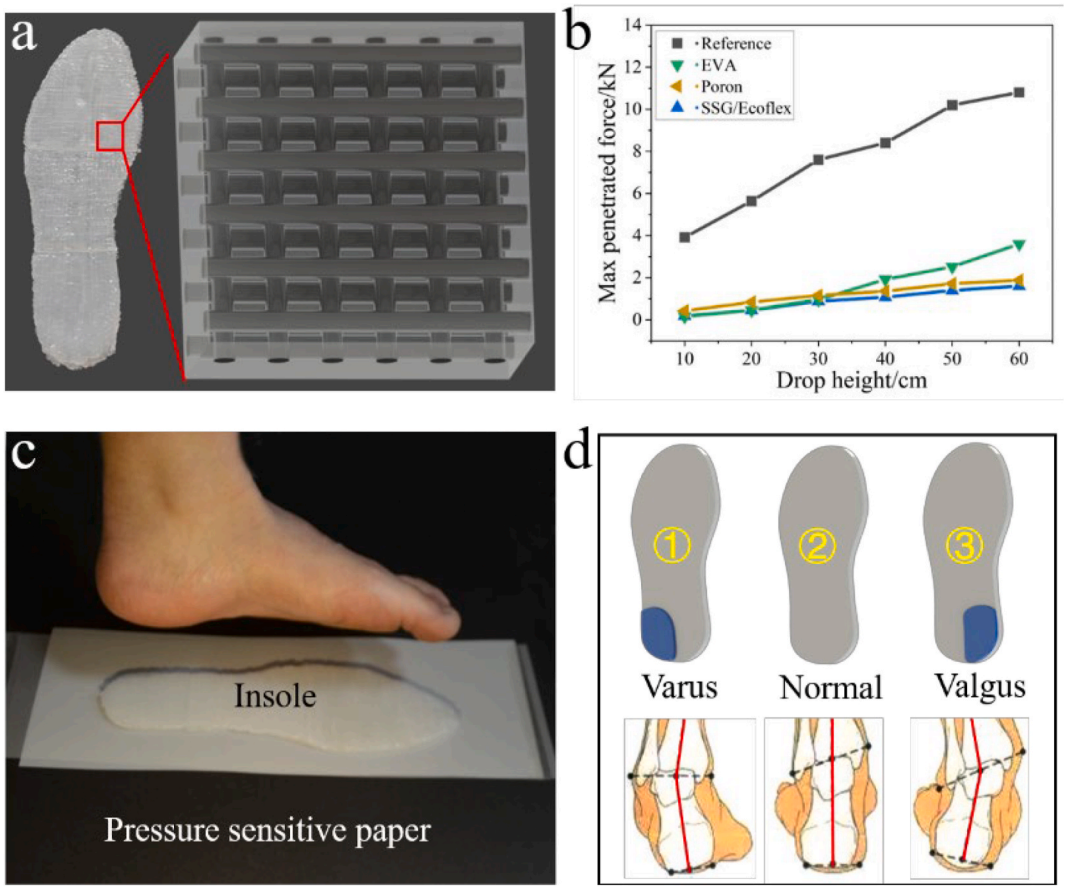

Fig. 8. The image of the SSG/Ecoflex hybrid three-layer insole and the schematic diagram of printing direction of three layers (a). The max penetrated force of different insoles (b). The image of the plantar pressure map test (c). The customized insoles and the images of varus, normal and valgus foot (d). The red lines presented the manners of the foot bearing the human body weight. The insole ② was flat and could be used for normal foot. Additional two layers (blue part) were printed on the outer or inner side of the heel of the insole ① or ③, which could be used for correcting varus and valgus foot, respectively. (For interpretation of the references to colour in this figure legend, the reader is referred to the Web version of this article.)

$$buffer\ ratio = 1 - F/F_R \quad (1)$$

where F was the penetrated force of the insole, and F_R was the penetrated force without the insole. The larger the buffer ratio, the better the protection performance. The buffer ratio of EVA foam insole reached 96% under a 10 cm drop height and reduced quickly to only 67% as the drop height rose to 50 cm (Fig. S5). Poron foam insoles exhibited a smaller buffer ratio of 89% under low-speed impact compared with EVA foam, while its protection effect attenuation with the drop height was much weaker. At a drop height of 50 cm, the buffer ratio was reduced to 83%, indicating better cushioning protection under intense exercises of Poron foam insoles. Due to the unique rate-dependent mechanical properties of SSG, SSG/Ecoflex hybrid insoles could provide outstanding cushioning effect under low-speed and high-speed impacts. At a drop height of 10 cm, the buffer ratio reached 95%, which was similar to EVA foam insoles. Increasing the drop height to 50 cm, the buffer ratio could still reach 85%, slightly better than Poron foam insoles. The above results indicated SSG/Ecoflex hybrid insoles could not only adapt to the

low-speed movement of the human body, such as walking but also performed well at high-speed sports, such as soccer, basketball, presenting broad application prospects in the field of body protection.

As the basic human movements, walking requires the cooperation of many systems to enable a person to walk forward with a normal and stable gait. Abnormal gait refers to the uncoordinated, unstable and discontinuous walking style of walking, indicating the imbalance of the human body and possible pathological features. Incorrect walking style is prone to wear joints, strain the muscles and may be related to nervous system problems sometimes [55,56]. The foot arch is the most important factors for walking gait. The normal foot arch can bear the pressure of the human body reasonably, cushion the impact and vibration, and protect the nerves and blood vessels of the foot from compression. For a normal arch, the center of the sole is tilted inward about 30°. Varus and valgus foot mean that the sole deflects to the inside and outside, which will lead to poor foot flexibility, lateral ankle instability, and sprain. It may also result in limited functionality of the arch, thus the athletic ability is restricted and the function of walking, running and jumping is weakened. Therefore, the timely diagnosis and physical correction of abnormal gait (such as varus and valgus foot) are very important to improve human health.

The plantar pressure test, which measured the upward force on the soles, was a kind of widely used and effective method to assess the state of walking function. The pressure sensitive paper, which could turn red as compressed, was used to record the plantar pressure (Fig. 8c). By using the programmable and scalable advantages of the coaxial DIW technique, the customized insole ① and insole ③ were prepared for correcting varus and valgus foot (Fig. 8d).

Fig. S6 presented the plantar pressure distribution of a standing volunteer with a normal arch and a weight of about 49 kg. The stressed region appeared red and the deeper the red, the greater the pressure. The Matlab software was used to process the original images to obtain the plantar pressure map (Fig. 9). Without insoles, the plantar pressure was pretty large, and mainly located at the forefoot, arch and back heel (Fig. 9a). The excessive pressure on the arch would lead to the decrease of cushioning effect, which may cause joint wear and even damage when exercising. Besides, the elasticity of the arch was reduced, declining the bounce ability. As insoles were applied, plantar pressure was reduced significantly. Due to the soft and elastic nature of insoles, they deformed and fitted the shape of the foot sole under the weight of the human body, thereby dispersing the pressure effectively. Because the pressure detection limit of pressure-sensitive paper was 0.05 MPa, the pressure in marginal areas was too low to detect, resulting in the reduction of the plantar pressure map area. Besides, the insole could effectively reduce the pressure on the arch, which not only protected the arch but also benefited its normal function. Compared with SSG/Ecoflex hybrid insole (insole ②), EVA foam and Poron foam insoles exhibited almost no difference in protective effects.

Due to the varus foot, the plantar pressure was concentrated on the outside and the arch was under excessive pressure (Fig. 10a). EVA and Poron foam insoles could reduce plantar pressure to a certain extent, but were unable to improve the situation of overlarge arch pressure (Fig. 10b and c). The insole ① could force the foot to reverse outward owing to two additional layers of SSG/Ecoflex hybrid films at the outer side of the insole heel. As insole ① was applied, not only the plantar pressure was reduced, but also the excessive pressure on the arch was relieved significantly due to the physical correction of the varus foot.

At the valgus foot, the plantar pressure was concentrated on the inner side and the arch was not stressed (Fig. 11a). In this case, the arch collapsed, which may cause the fibula to collide with the calcaneus during walking. Similarly, EVA and Poron foam insoles reduced plantar pressure effectively but were powerless to improve the valgus foot (Fig. 11 b, c). The insole ③ was applied to force the foot to reverse inward by adding two additional layers of SSG/Ecoflex hybrid film at the inner side of the insole heel (Fig. 11d). The insole ③ alleviated the foot valgus and the outside of the sole also shared part of the body pressure. At the same time, it greatly reduced the plantar pressure and protected the skin and tissues of the feet.

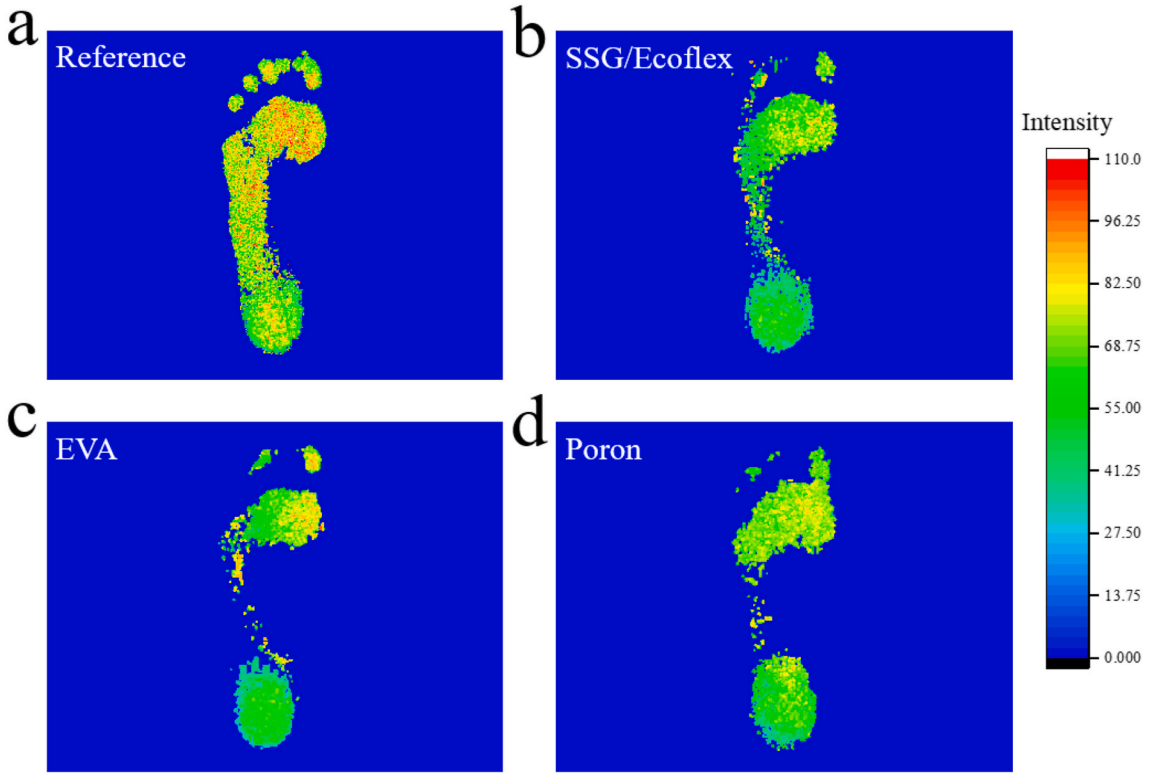

Fig. 9. The plantar pressure map of the normal arch. The plantar pressure map without insole (a), with the protection of SSG/Ecoflex hybrid (b), EVA foam (c), Poron foam (d) insoles. The insole ② was used here.

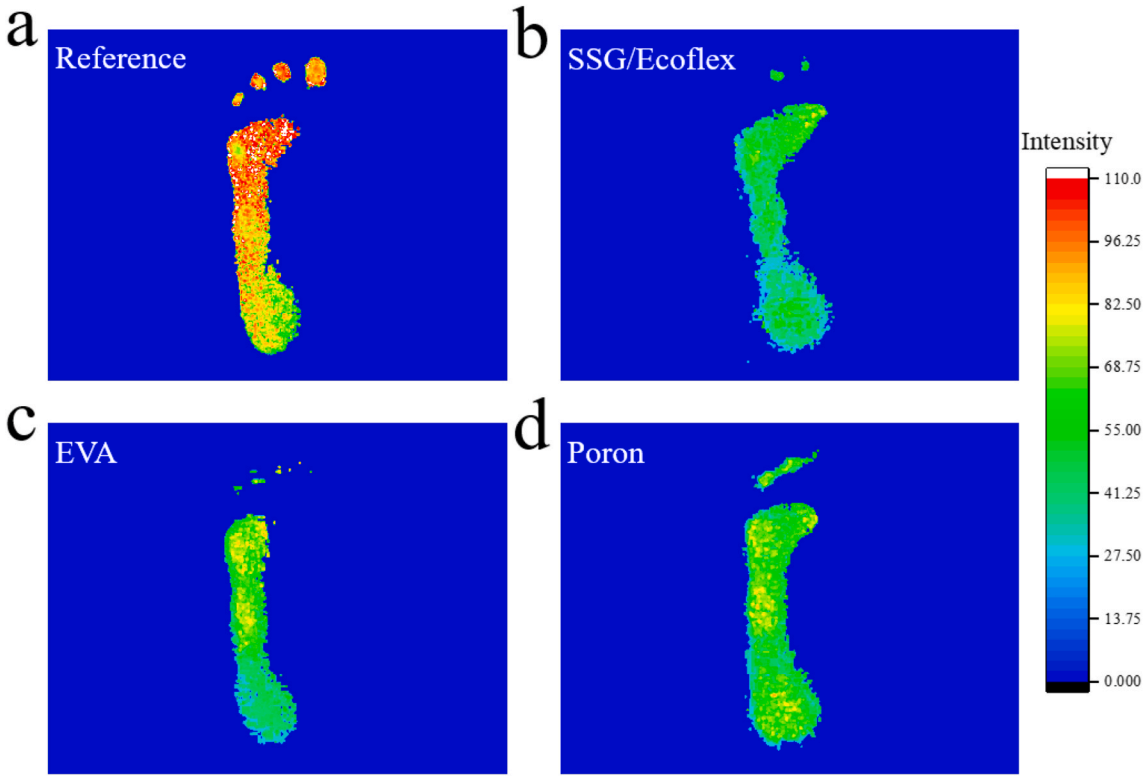

Fig. 10. The plantar pressure map of varus foot. The plantar pressure map without insole (a), with the protection of SSG/Ecoflex hybrid (b), EVA foam (c), Poron foam (d) insole. The insole ① was used here.

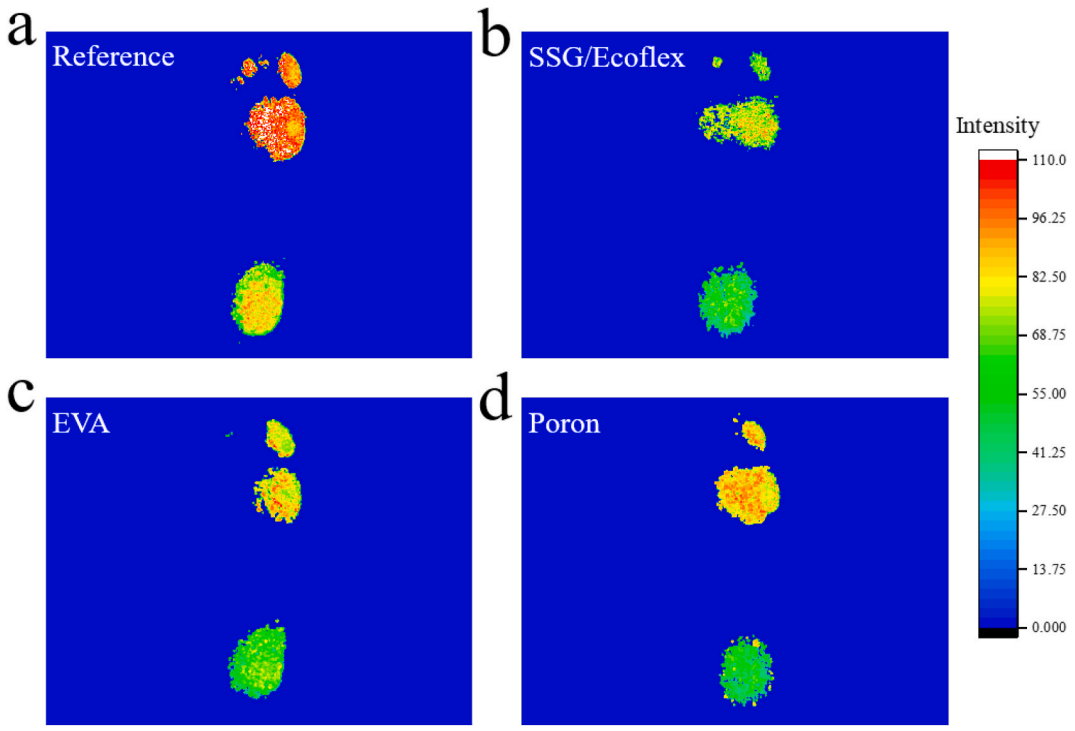

Fig. 11. The plantar pressure map of valgus foot. The plantar pressure map without insole (a), with the protection of SSG/Ecoflex hybrid (b), EVA foam (c), Poron foam (d) insole. The insole ③ was used here.

4. Conclusion

In summary, we demonstrated a simple and efficient coaxial DIW method to construct SSG/Ecoflex composite based customer-fit insoles, which could protect against dynamic shocks during exercising and physical correction to abnormal walking gait simultaneously. The inner printing ink SSG exhibited typical rate-dependent mechanical property with storage modulus rising 3 orders of magnitude with the shear

frequency. The printing direction resulted in the tensile anisotropy of SSG/Ecoflex hybrid films, which could be eliminated by designing the printing direction of double-layer films. Due to the rate-dependent property of inner SSG, the films could dissipate 53.4% impact acceleration, 46.9% penetrated force and increase buffer time by 1.6 times under dynamic loadings, presenting excellent safeguarding performance. Besides, the SSG/Ecoflex hybrid insoles provided more effective protection during both mild and violent exercising compared with commercial insoles. Finally, with the help of scalable and programmable coaxial DIW technique, the customer-fit insoles were fabricated which benefited the abnormal walking gait correction, such as varus and valgus foot. Therefore, the coaxial additive manufacture technique for constructing SSG/Ecoflex composite based sports armors showed broad application prospections in future safeguarding and foot orthopedics areas. More importantly, more advanced sports armors that take the advantages both from the fabrication customization superiority of coaxial DIW technique and the outstanding safeguarding function of SSG would be a possible solution for emerging personalized sports safety and health improvement needs.

Credit authorship contribution statement

Shuaishuai Zhang performed all the experiments and wrote the draft of the manuscript. Liang Lu, Sheng Wang, Shouhu Xuan, and Xinglong Gong revised and discussed the manuscript. Shuaishuai Zhang, Fang Yang carried out the plantar pressure tests. Liang Lu provided advices for waking gait monitoring tests and related data analysis.

Declaration of competing interest

The authors declare that they have no known competing financial interests or personal relationships that could have appeared to influence the work reported in this paper.

Acknowledgements

Financial supports from the National Natural Science Foundation of China (Grant No. 11822209, 12072338, 11802303, 11772320, 12132016), the Fundamental Research Funds for the Central Universities (WK2480000007), and the Strategic Priority Research Program of the Chinese Academy of Sciences (Grant No. XDB22040502) were gratefully acknowledged.

Appendix A. Supplementary data

Supplementary data to this article can be found online at https://doi.org/10.1016/j.compositesb.2021.109268.

References

[1] Zwingmann L, Hoppstock M, Goldmann JP, Wahl P. The effect of physical training modality on exercise performance with police-related personal protective equipment. Appl Ergon 2021;93:103371.
[2] Takata Y, Matsuoka S, Okumura N, Iwamoto K, Takahashi M, Uchiyama E. Standing balance on the ground -The influence of flatfeet and insoles. J Phys Ther Sci 2013;25(12):1519–21.
[3] Lavender SA, Wang Z, Allread WG, Sommerich CM. Quantifying the effectiveness of static and dynamic insoles in reducing the tibial shock experienced during walking. Appl Ergon 2019;74:118–23.
[4] Qin J, Guo B, Zhang L, Wang T, Zhang G, Shi X. Soft armor materials constructed with Kevlar fabric and a novel shear thickening fluid. Composites, Part B 2020;183:107686.
[5] Xu C, Wang Y, Wu J, Song S, Cao S, Xuan S, et al. Anti-impact response of Kevlar sandwich structure with silly putty core. Compos Sci Technol 2017;153:168–77.
[6] Wang S, Xuan S, Liu M, Bai L, Zhang S, Sang M, et al. Smart wearable Kevlar-based safeguarding electronic textile with excellent sensing performance. Soft Matter 2017;13(13):2483–91.
[7] Wang S, Gong L, Shang Z, Ding L, Yin G, Jiang W, et al. Novel safeguarding tactile e-skins for monitoring human motion based on SST/PDMS-AgNW-PET hybrid structures. Adv Funct Mater 2018;28(18):1707538.
[8] Zhao C, Xu C, Cao S, Xuan S, Jiang W, Gong X. Anti-impact behavior of a novel soft body armor based on shear thickening gel (STG) impregnated Kevlar fabrics. Smart Mater Struct 2019;28(7):075036.
[9] Jiang W, Gong X, Wang S, Chen Q, Zhou H, Jiang W, et al. Strain rate-induced phase transitions in an impact-hardening polymer composite. Appl Phys Lett 2014;104(12):1100.
[10] Zhao C, Wang Y, Cao S, Xuan S, Jiang W, Gong X. Conductive shear thickening gel/Kevlar wearable fabrics: a flexible body armor with mechano-electric coupling ballistic performance. Compos Sci Technol 2019;182:107782.
[11] Wang Y, Ding L, Zhao C, Wang S, Xuan S, Jiang H, et al. A novel magnetorheological shear-stiffening elastomer with self-healing ability. Compos Sci Technol 2018;168:303–11.
[12] Wang S, Xuan S, Wang Y, Xu C, Mao Y, Liu M, et al. Stretchable polyurethane sponge scaffold strengthened shear stiffening polymer and its enhanced safeguarding performance. ACS Appl Mater Interfaces 2016;8(7):4946–54.
[13] Yuan F, Wang S, Zhang S, Wang Y, Xuan S, Gong X. A flexible viscoelastic coupling cable with self-adapted electrical properties and anti-impact performance toward shapeable electronic devices. J Mater Chem C 2019;7(27):8412–22.
[14] Sadeghpour A, Aslani H, Gojazadeh M, Pashazadeh M. The study of silicon shoes insert benefits in symptom and radiology of patients with idiopathic femoral head osteonecrosis: two arms randomized controlled trial. Crescent J Med Biol Sci 2020;7(1):104–9.
[15] Greitemann B, Schievink F. Orthopedic shoe technology. Rehabilitation 2021;60:45–66. 01.
[16] Wu X, Su Y, Shi J. Perspective of additive manufacturing for metamaterials development. Smart Mater Struct 2019;28(9):093001.
[17] Cohn D, Zarek M, Elyashiv A, Abu Sbitan M, Sharma V, Ramanujan RV. Remotely triggered morphing behavior of additively manufactured thermoset polymer-magnetic nanoparticle composite structures. Smart Mater Struct 2021;30(4):045022.
[18] Da Cruz Gomes AA, Grassi END, da Silva PCS, de Araujo CJ. Mechanical behavior of a NiTi superelastic bone plate obtained by investment casting assisted by additive manufacturing. Smart Mater Struct 2021;30(2):025009.
[19] Ghimire A, Tsai YY, Chen PY, Chang SW. Tunable interface hardening: designing tough bio-inspired composites through 3D printing, testing, and computational validation. Composites, Part B 2021;215:108754.
[20] Watschke H, Goutier M, Heubach J, Vietor T, Leichsenring K, Boel M. Novel resistive sensor design utilizing the geometric freedom of additive manufacturing. Appl Sci 2021;11(1):113.
[21] Leigh SJ, Purssell CP, Billson DR, Hutchins DA. Using a magnetite/thermoplastic composite in 3D printing of direct replacements for commercially available flow sensors. Smart Mater Struct 2014;23(9):095039.
[22] Herren B, Saha MC, Altan MC, Liu Y. Development of ultrastretchable and skin attachable nanocomposites for human motion monitoring via embedded 3D printing. Composites, Part B 2020;200:108224.
[23] Wang J, Shao C, Wang Y, Sun L, Zhao Y. Microfluidics for medical additive manufacturing. Engineering 2020;6(11):1244–57.
[24] Vyatskikh A, Ng RC, Edwards B, Briggs RM, Greer JR. Additive manufacturing of high-refractive-index, nanoarchitected titanium dioxide for 3D dielectric photonic crystals. Nano Lett 2020;20(5):3513–20.
[25] Bose S, Vahabzadeh S, Bandyopadhyay A. Bone tissue engineering using 3D printing. Mater Today 2013;16(12):496–504.
[26] Liu K, Li W, Chen S, Wen W, Lu L, Liu M, et al. The design, fabrication and evaluation of 3D printed gHNTs/gMgO whiskers/PLLA composite scaffold with honeycomb microstructure for bone tissue engineering. Composites, Part B 2020;192:108001.
[27] Mohammed A, Elshaer A, Sareh P, Elsayed M, Hassanin H. Additive manufacturing technologies for drug delivery applications. Int J Pharm (Amst) 2020;580:119245.
[28] Konasch J, Riess A, Mau R, Teske M, Rekowska N, Eickner T, et al. A novel hybrid additive manufacturing process for drug delivery systems with locally incorporated drug depots. Pharmaceutics 2019;11(12):661.
[29] Lazarus N, Bedair SS. Creating 3D printed sensor systems with conductive composites. Smart Mater Struct 2021;30(1):015020.
[30] Celestine ADN, Agrawal V, Runnels B. Experimental and numerical investigation into mechanical degradation of polymers. Composites, Part B 2020;201:108369.
[31] Ji J, Wang M, Hu M, Mao L, Wang Q, Zhou W, et al. 3D-printing AIE stereolithography resins with real-time monitored printing process to fabricate fluorescent objects. Composites, Part B 2021;206:108526.
[32] Le Duigou A, Chabaud G, Matsuzaki R, Castro M. Tailoring the mechanical properties of 3D-printed continuous flax/PLA biocomposites by controlling the slicing parameters. Composites, Part B 2020;203:108474.
[33] Cho YS, Son SJ, Kim YK, Chung KC, Choi CJ. Development of direct ink writing technology for micro-structures. Rev Adv Mater Sci 2011;28(2):175–80.
[34] Brilian AI, Soum V, Park S, Lee S, Kim J, Kwon K, et al. A simple route of printing explosive crystalized micro-patterns by using direct ink writing. Micromachines 2021;12(2):105.
[35] Rocha VG, Saiz E, Tirichenko IS, Garcia-Tunon E. Direct ink writing advances in multi-material structures for a sustainable future. J Mater Chem 2020;8(31):15646–57.
[36] Wang H, Liu Z, Ding J, Lepro X, Fang S, Jiang N, et al. Downsized sheath-core conducting fibers for weavable superelastic wires, biosensors, supercapacitors, and strain sensors. Adv Mater 2016;28(25):4998–5007.
[37] Hu T, Xuan S, Ding L, Gong X. Liquid metal circuit based magnetoresistive strain sensor with discriminating magnetic and mechanical sensitivity. Sens Actuators, B 2020;314:128095.

[38] Zhang Y, Zhang W, Ye G, Tan Q, Zhao Y, Qiu J, et al. Core-sheath stretchable conductive fibers for safe underwater wearable electronics. Adv Mater Technol 2020;5(1):1900880.
[39] Wei X, Liu C, Wang Z, Luo Y. 3D printed core-shell hydrogel fiber scaffolds with NIR-triggered drug release for localized therapy of breast cancer. Int J Pharm (Amst) 2020;580:119219.
[40] Shao L, Gao Q, Xie C, Fu J, Xiang M, He Y. Directly coaxial 3D bioprinting of large-scale vascularized tissue constructs. Biofabrication 2020;12(3):035014.
[41] Gu Z, Fu J, Lin H, He Y. Development of 3D bioprinting: from printing methods to biomedical applications. Asian J Pharm Sci 2020;15(5):529–57.
[42] Liu X, Carter SSD, Renes MJ, Kim J, Rojas Canales DM, Penko D, et al. Development of a coaxial 3D printing platform for biofabrication of implantable islet-containing constructs. Adv Healthcare Mater 2019;8(7):1801181.
[43] Khondoker MAH, Ostashek A, Sameoto D. Direct 3D printing of stretchable circuits via liquid metal co-extrusion within thermoplastic filaments. Adv Eng Mater 2019;21(7):1900060.
[44] Zhao J, Lu H, Zhang Y, Yu S, Malyi OI, Zhao X, et al. Direct coherent multi-ink printing of fabric supercapacitors. Sci Adv 2021;7(3):eabd6978.
[45] Zhao J, Lu H, Zhao X, Malyi OI, Peng J, Lu C, et al. Printable ink design towards customizable miniaturized energy storage devices. ACS Mater Lett 2020;2(9):1041–56.
[46] Zhao J, Zhang Y, Zhao X, Wang R, Xie J, Yang C, et al. Direct ink writing of adjustable electrochemical energy storage device with high gravimetric energy densities. Adv Funct Mater 2019;29(26):1900809.
[47] Lu H, Peng Q, Wang Z, Zhao J, Zhang X, Meng L, et al. 3D printing coaxial fiber electrodes towards boosting ultralong cycle life of fibrous supercapacitors. Electrochim Acta 2021;380:138220.
[48] Wang S, Xuan S, Jiang W, Jiang W, Yan L, Mao Y, et al. Rate-dependent and self-healing conductive shear stiffening nanocomposite: a novel safe-guarding material with force sensitivity. J Mater Chem 2015;3(39):19790–9.
[49] Wang Y, Wang S, Xu C, Xuan S, Jiang W, Gong X. Dynamic behavior of magnetically responsive shear-stiffening gel under high strain rate. Compos Sci Technol 2016;127:169–76.
[50] Lombardi L, Tammaro D. Effect of polymer swell in extrusion foaming of low-density polyethylene. Phys Fluids 2021;33(3):033104.
[51] Riou M, Ausias G, Grohens Y, Gaudry T, Veille JM, Ferec J. Thermoplastic foaming with thermo-expandable microcapsules: mathematical modeling and numerical simulation for extrusion process. Chem Eng Sci 2020;227:115852.
[52] Zhou J, Wang S, Yuan F, Zhang J, Liu S, Zhao C, et al. Functional Kevlar-based triboelectric nanogenerator with impact energy-harvesting property for power source and personal safeguard. ACS Appl Mater Interfaces 2021;13(5):6575–84.
[53] Bittencourt NFN, Meeuwisse WH, Mendonca LD, Nettel AA, Ocarino JM, Fonseca ST. Complex systems approach for sports injuries: moving from risk factor identification to injury pattern recognition-narrative review and new concept. Br J Sports Med 2016;50(21):1309.
[54] Gabbett TJ. Debunking the myths about training load, injury and performance: empirical evidence, hot topics and recommendations for practitioners. Br J Sports Med 2020;54(1):58–66.
[55] Gaffney BMM, Van Dillen LR, Foody JN, Burnet PE, Clohisy JC, Chen L, et al. Multi-joint biomechanics during sloped walking in patients with developmental dysplasia of the hip. Clin Biomech 2021;84:105335.
[56] Kegelmeyer DA, Kostyk SK, Fritz NE, Scharre DW, Young GS, Tan Y, et al. Immediate effects of treadmill walking in individuals with Lewy body dementia and Huntington's disease. Gait Posture 2021;86:186–91.